

The initial evolution of millisecond magnetars: an analytical solution

S. Çikintoğlu¹★, S. Şaşmaz Muş¹, K. Yavuz Ekşi¹

¹*Istanbul Technical University, Faculty of Science and Letters, Physics Engineering Department, 34469, Istanbul, Turkey*

Accepted XXX. Received YYY; in original form ZZZ

ABSTRACT

Millisecond magnetars are often invoked as the central engine of some gamma-ray bursts (GRBs), specifically the ones showing a plateau phase. We argue that an apparent plateau phase may not be realized if the magnetic field of the nascent magnetar is in a transient rapid decay stage. Some GRBs that lack a clear plateau phase may also be hosting millisecond magnetars. We present an approximate analytical solution of the coupled set of equations describing the evolution of the angular velocity and the inclination angle between rotation and magnetic axis of a neutron star in the presence of a co-rotating plasma. We also show how the solution can be generalized to the case of evolving magnetic fields. We determine the evolution of the spin period, inclination angle, magnetic dipole moment and braking index of six putative magnetars associated with GRB 091018, GRB 070318, GRB 080430, GRB 090618, GRB 110715A, GRB 140206A through fitting, via Bayesian analysis, the X-ray afterglow light curves by using our recent model [Şaşmaz Muş et al. 2019]. We find that within the first day following the formation of the millisecond magnetar, the inclination angle aligns rapidly, the magnetic dipole field may decay by a few times and the braking index varies by an order of magnitude.

Key words: gamma-ray burst: general – stars: magnetars

1 INTRODUCTION

Gamma-ray bursts (GRBs) are highly energetic explosions with durations of milliseconds to minutes (Lyutikov & Blandford 2003; Zhang & Mészáros 2004; Piran 2005; Kumar & Zhang 2015). The prompt emission is followed by an X-ray afterglow (Costa et al. 1997). It is considered that the central engine of some of the GRBs could be strongly magnetized rapidly spinning neutron stars, i.e. millisecond magnetars (Usov 1992; Duncan & Thompson 1992), specifically the ones showing a plateau stage in their afterglows (Dai & Lu 1998a,b). The spin-down power of a millisecond magnetar, $L_{\text{sd}} = -I\dot{\Omega}$ where I is the moment of inertia of the star, Ω is the angular velocity, and the dot denotes the derivative with respect to time, is employed for explaining the X-ray afterglows:

$$L_X = \eta L_{\text{sd}}, \quad (1)$$

where η is an efficiency coefficient. In the case of spin-down under magnetic dipole torque $I\dot{\Omega} = -2\mu^2 \sin^2 \alpha \Omega^3 / 3c^3$ where μ is the magnetic dipole moment and α is the inclination angle between rotation and magnetic axis, an exact analytic

solution, $\Omega = \Omega_0(1 + t/t_0)^{-1/2}$, can be obtained where Ω_0 is the initial angular velocity and $t_0 = 3Ic^3/(2\mu\Omega_0 \sin \alpha)^2$ is the spin-down time-scale. This leads to $L_X = \eta L_0(1 + t/t_0)^{-2}$ where $L_0 = 2\mu^2\Omega_0^4 \sin^2 \alpha / 3c^3$. The spin-down time-scale t_0 determines the duration of the plateau phase which is followed by the rapid-decay stage $L_X \propto t^{-2}$. This model has been generalized by Lasky et al. (2017) to infer the braking indices of nascent magnetars (see also Lü et al. 2019).

The solution given above, employed by many previous work, neglects the alignment component of the dipole torque (Michel & Goldwire 1970; Davis & Goldstein 1970). It also assumes a constant magnetic dipole moment rotating in vacuum. Initially, the magnetar is far from an equilibrium stage and its just generated magnetic field may be in a rapid relaxation stage (Geppert & Rheinhardt 2006; Beniamini et al. 2017). Because of this rapid decay of the field, the spin-down power may decline so fast that a clear ‘plateau phase’ may not be realized.

In this work we employ the recent model proposed by Şaşmaz Muş et al. (2019) (hereafter Paper I) for modeling the X-ray afterglows of six putative magnetars associated with GRB afterglow light curves, GRBs 091018, 070318, 080430, 090618, 110715A and 140206A. This model assumes the magnetar has a corotating plasma (Goldreich & Julian

★ E-mail: cikintoglus@itu.edu.tr

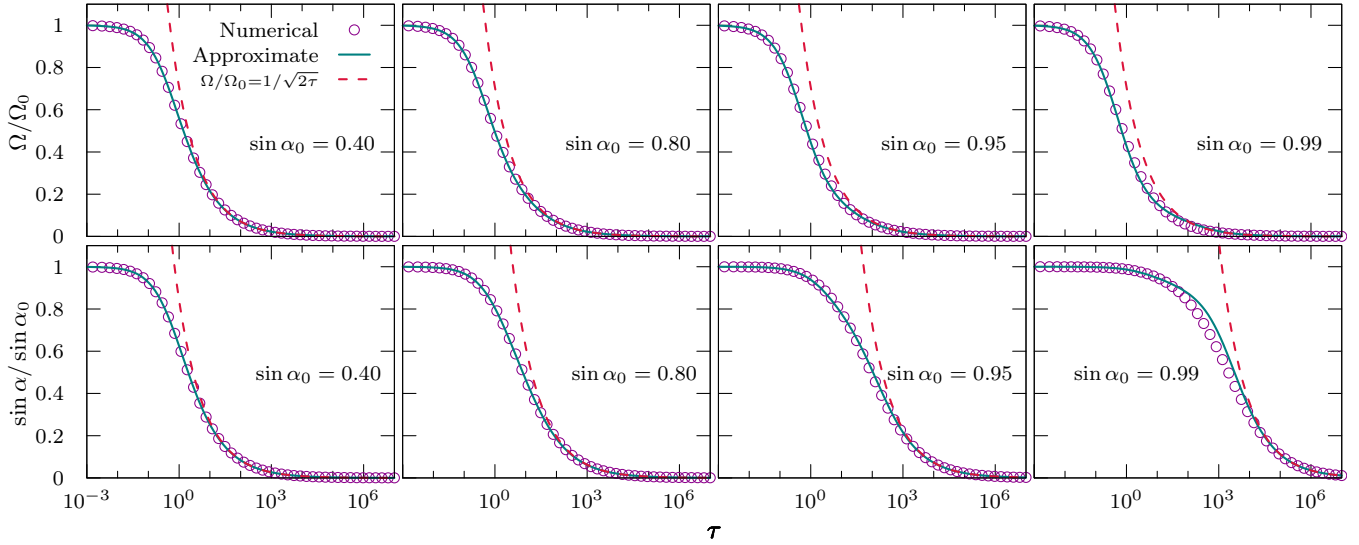


Figure 1. The evolution of angular velocity (**upper panels**) and inclination angle (**lower panels**) for various initial angles. The circles denote the numerical solutions, the solid lines denote the approximate analytical solutions given in Equations (13)-(15) and the dashed lines (red in electronic version) represent the late-time limits given in Equation (18). The time in the x-axis is in units of spin-down time scale defined in Eqn. 9.

1969) and employs the appropriate spin-down (Spitkovsky 2006) and alignment (Philippov et al. 2014) torque components. It also assumes an exponential relaxation of the magnetic dipole moment (Paper I).

We review the model equations in Section 2.1. We present an approximate analytical solution for the model equations in Section 2.2, GRB sample used in this work in Section 2.3 and the method for fitting the model to the GRB afterglow light curves in Section 2.4. We present our results in Section 3 and discuss the implications of our findings in Section 4.

2 METHOD

2.1 Model equations

We employ the model recently set-up by Paper I to fit the X-ray afterglow light curves of 7 GRBs. This model is a set of three ordinary differential equations (ODEs) which employs the spin-down (Spitkovsky 2006)

$$I \frac{d\Omega}{dt} = -\frac{\mu^2 \Omega^3}{c^3} (1 + \sin^2 \alpha), \quad (2)$$

and alignment (Philippov et al. 2014)

$$I \frac{d\alpha}{dt} = -\frac{\mu^2 \Omega^2}{c^3} \sin \alpha \cos \alpha, \quad (3)$$

components of the magnetic dipole torque in the presence of a corotating plasma (Hones & Bergeson 1965; Goldreich & Julian 1969), and a simple prescription for the evolution of the magnetic dipole moment

$$\dot{\mu} = -(\mu - \mu_\infty)/t_m, \quad (4)$$

(Paper I) where μ_∞ is the settling value of the magnetic dipole moment and t_m is its evolution time-scale. This model

Table 1. Redshift and photon indices of the GRB sample^a.

GRB	Redshift z	Photon Index Γ
091018	0.971	2.0 ± 0.115
070318	0.84	2.01 ± 0.12
080430	0.767	1.98 ± 0.09
090618	0.54	1.83 ± 0.04
110715A	0.82	1.760 ± 0.105
140206A	2.73	1.80 ± 0.05

^aRedshifts and photon indices are obtained from the Swift/*XRT* GRB light curve repository (Evans et al. 2007, 2009).

predicts the braking index to be

$$n \equiv \frac{\Omega \ddot{\Omega}}{\dot{\Omega}^2} = 3 + 2 \left[\frac{\sin \alpha \cos \alpha}{1 + \sin^2 \alpha} \right]^2 + 2 \frac{\Omega}{\dot{\Omega}} \frac{\dot{\mu}}{\mu}. \quad (5)$$

The first two equations, Eqn.(2) and Eqn.(3), are coupled while Equation (4) can be solved independently to give

$$\mu = \mu_\infty + (\mu_0 - \mu_\infty) e^{-t/t_m}, \quad (6)$$

where μ_0 is the initial magnetic dipole moment of the magnetar.

2.2 Approximate analytical solutions of the angular velocity and inclination angle

In Paper I we have solved the above set of equations numerically to find the evolution of Ω , α and thus L_X . Although a single numerical solution takes less than a second, the Bayesian fitting procedure coupled with the MCMC simulation, requires solving the ODE set several hundred thousand times which is computationally expensive. An exact solution for Equations (2) and (3) is given in Philippov et al. (2014),

Table 2. Estimated values of the putative nascent magnetar parameters for the changing magnetic dipole moment case.

GRB	P_0 (ms)	$\sin \alpha_0$	μ_0 (10^{33} G cm 3)	μ_∞ (10^{33} G cm 3)	t_m (days)	χ^2/dof
091018	2.917 ± 0.041	0.488 ± 0.221	1.829 ± 0.167	0.689 ± 0.063	0.015 ± 0.002	139.35/134
091018 ^a	2.922 ± 0.039	0.523 ± 0.236	1.804 ± 0.170	0.683 ± 0.063	0.016 ± 0.002	139.23/134
070318	3.848 ± 0.064	0.454 ± 0.226	1.382 ± 0.127	0.369 ± 0.038	0.024 ± 0.002	126.90/90
080430	4.237 ± 0.070	0.547 ± 0.200	0.442 ± 0.043	0.233 ± 0.030	0.158 ± 0.057	140.42/140
090618	2.570 ± 0.014	0.709 ± 0.082	0.653 ± 0.028	0.374 ± 0.019	0.068 ± 0.008	1188.64/975
110715A	1.913 ± 0.021	0.408 ± 0.211	0.860 ± 0.069	0.179 ± 0.016	0.023 ± 0.001	362.53/248
140206A	0.670 ± 0.008	0.628 ± 0.243	0.264 ± 0.030	0.119 ± 0.014	0.037 ± 0.002	594.17/479

^a Parameter values obtained from numerical analysis presented in [Paper I](#).

but as this solution is implicit, employing it would require solving the algebraic equation numerically at each time step, therefore, using this method does not improve the computational expense.

We, thus, present a very accurate approximate solution of the angular velocity and inclination angle, i.e. the ODE set in Section 2.1. This significantly (by ~ 5 times) reduces the computational time and gives insight into the dependencies of the spin and inclination angle.

Equations (2)-(3) implies an integration constant

$$\Omega \frac{1 - \sin^2 \alpha}{\sin \alpha} = \Omega_0 \frac{1 - \sin^2 \alpha_0}{\sin \alpha_0}, \quad (7)$$

where Ω_0 and α_0 are the initial values of the spin and the inclination angle, respectively ([Philippov et al. 2014](#)). By using the integration constant, the angular velocity can be eliminated from Equation (3),

$$\frac{dy}{d\tau} = -\frac{y^3}{1-y^2} \frac{(1-y_0^2)^2}{y_0^2}, \quad (8)$$

where $y = \sin \alpha$, $y_0 = \sin \alpha_0$ and the dimensionless time, τ , is defined as

$$\tau \equiv \frac{\Omega_0^2}{Ic^3} \int_0^t \mu^2 dt. \quad (9)$$

Integrating Equation (8) gives

$$-y_0^2 \ln(1 + \xi) + \xi = 2(1 - y_0^2)^2 \tau, \quad (10)$$

where $\xi = y_0^2/y^2 - 1$. By applying the approximate solution,

$$\xi = \xi_0 + y_0^2 \xi_1 + y_0^4 \xi_2, \quad (11)$$

into Equation (10) and then solving it to the order of y_0 , an approximate solution for the inclination angle is obtained as

$$y(\tau) = \frac{y_0}{\sqrt{1 + 2(1 - y_0^2)^2 \tau + y_0^2 \ln(1 + 2\tau) + y_0^4 \frac{\ln(1+2\tau) - 4\tau}{1+2\tau}}}. \quad (12)$$

If y_0 is zero or one, Equation (8) implies trivially $y(\tau) = y_0$. Equation (12) yields the former case, yet, it does not yield the latter one. This can be fixed by modifying the solution as

$$y(\tau) = \frac{y_0}{\sqrt{1 + f(\tau)}}, \quad (13)$$

where

$$f(\tau) = 2(1 - y_0^2)^2 \tau + y_0^2 \ln(1 + 2\tau) + y_0^4 \frac{\ln(1 + 2\tau) - 4\tau}{1 + 2\tau} - y_0^8 \left(\ln(1 + 2\tau) + \frac{\ln(1 + 2\tau) - 4\tau}{1 + 2\tau} \right). \quad (14)$$

The spin evolution can be easily obtained from Equation (7)

$$\Omega(\tau) = \Omega_0 \left(1 - y_0^2 \right) \frac{\sqrt{1 + f(\tau)}}{1 - y_0^2 + f(\tau)}. \quad (15)$$

These approximate solutions are well-consistent with the numerical solutions as shown in [Figure 1](#). The relative difference between the approximate solution and numerical solution is less than 6% for $\alpha_0 < 70^\circ$. Also, the form of the solutions is not altered in the case of changing magnetic field as the field evolution only modifies the relation between the time, t , and the dimensionless time, τ given in Equation (9).

The linear term of τ increases faster than the logarithmic term $\ln(1 + \tau)$. So, in the limit of $\tau \gg 1$, the approximate solution of the inclination angle reduces to

$$y(\tau) \simeq \frac{y_0}{\sqrt{1 + 2(1 - y_0^2)^2 \tau}}, \quad (16)$$

as well as the spin of the star reduces to

$$\Omega(\tau) \simeq \Omega_0 \frac{1 - y_0^2}{\sqrt{1 + 2(1 - y_0^2)^2 \tau}}. \quad (17)$$

For later times, $\tau \gg 1/(1 - y_0^2)^2$, both the inclination angle and the spin of the star approximate to

$$y(\tau) \simeq \frac{y_0}{(1 - y_0^2)\sqrt{2\tau}}, \quad \text{and} \quad \Omega(\tau) \simeq \frac{\Omega_0}{\sqrt{2\tau}}. \quad (18)$$

Accordingly, both the spin and the inclination angle decrease with $\tau^{-1/2}$ for the late time. The magnetic field and the rotation axis almost aligned ($\alpha < 11^\circ$) in this limit. If the magnetic field is constant, this limit indicates a time-scale

$$t_{\text{alignment}} \sim 10^{-1} \frac{y_0^2}{(1 - y_0^2)^2} \frac{I_{45}}{\mu_{33}^2} \left(\frac{P_0}{1 \text{ ms}} \right)^2 \text{ day}, \quad (19)$$

where $I_{45} = I/10^{45}$ g cm 2 and $\mu_{33} = \mu/10^{33}$ G cm 3 . Alignment takes longer if the magnetic field decreases with time.

2.3 GRB sample

Our sample in this work contains GRBs 070318, 080430, 090618, 110715A, 140206A and 091018. We included GRB 091018, a source which is also presented in [Paper I](#), in order to compare the numerical and approximate analytical solutions.

In contrast to [Paper I](#), we did not restrict our sample only to GRBs with plateau phases since we now have clue that the magnetic dipole moment might be changing in the first day of a nascent magnetar. Thus, it is possible to model GRB afterglow light curves with steeper evolution.

The unabsorbed flux values, redshifts and photon indices of the GRB sample are obtained from the Swift-XRT GRB light curve repository¹ ([Evans et al. 2007, 2009](#)) and listed in [Table 1](#). We converted the unabsorbed flux values, F_X , to luminosity values using

$$L = 4\pi d_L^2(z) F_X k(z). \quad (20)$$

Luminosity distance, $d_L(z)$, is calculated in a flat Λ CDM cosmological model using `astropy.cosmology` subpackage ([Price-Whelan et al. 2018](#)). The cosmological parameters are taken as $H_0 = 71 \text{ km s}^{-1} \text{ Mpc}^{-1}$ and $\Omega_M = 0.27$. The cosmological k -correction ([Bloom et al. 2001](#)), $k(z)$, is calculated with $k(z) = (1+z)^{(\Gamma-2)}$ using redshift and photon index (Γ) values listed in [Table 1](#) for each GRB.

2.4 Parameter estimation

We estimated the period, inclination angle, magnetic dipole moment of nascent magnetars at the start of the plateau phase as well as the value of the magnetic dipole moment which the star settles down and the evolution time-scale of this relaxation by using a Bayesian framework. We have given the details of this analysis in [Paper I](#). The light curves of the selected GRBs are modelled with

$$L_X = \eta \frac{\mu^2 \Omega^4}{c^3} (1 + \sin^2 \alpha). \quad (21)$$

Here, α and Ω are calculated using approximate analytical solutions presented in [Section 2.2](#) by Equations (13) and (15).

We used Gaussian log-likelihood and uniform prior probability to construct the posterior probability distribution with the same prior probabilities given in [Paper I](#) except for GRB 140206A. For this source we decreased the lower limit of the initial rotation period from 0.7 ms to 0.5 ms as initial analysis suggested a lower value for this source. Finally, we sampled the posterior probability distribution of the parameters with `emcee` ([Foreman-Mackey et al. 2013, 2018](#)) as described in [Paper I](#) in detail and obtained the parameter values from the posterior distributions of each parameters.

3 RESULTS

We have modelled the X-ray afterglow light curves of GRB 091018, GRBs 070318, 080430, 090618, 110715A and 140206A with the model described above to determine

the initial parameters of the putative magnetars with the Bayesian method introduced above. The estimated values of the putative nascent magnetar parameters of the selected GRBs are presented in [Table 2](#). The evolution as well as the 1D and 2D posterior distributions of the parameters are presented in [Figure 2](#), [Figure 3](#), [Figure 4](#), [Figure 5](#), [Figure 6](#) and [Figure 7](#), respectively. We included GRB 091018 in our data set to compare numeric solution presented in [Paper I](#) and analytic solution presented in this paper.

We have found that, within the time frame of the X-ray afterglow—about a few days following the birth of the magnetar—the inclination angle of putative magnetars change from $\sim 30^\circ$ – 40° to $\sim 5^\circ$ – 10° and the magnetic dipole moments decrease by a factor of 2–5. As a result, the braking index varies significantly in the episodes considered, confirming the previous results of [Paper I](#).

The initial periods and magnetic moments determined in this work depend on the choice of the efficiency factor η and moment of inertia I . The η parameter which involves the X-ray efficiency and the beaming factor varies in a wide range; it can be as low as 10^{-5} or high as 50 ([Frail et al. 2001; Kargaltsev et al. 2012](#)). In our simulations we fix η as 1, but below, we explain and display in [Figure 8](#) how the initial parameters transform for different values of η . The moment of inertia of a neutron star takes values around 10^{45} g cm^2 depending on the equation of state, the central mass density and the spin of the star ([Haensel et al. 2007](#)). In this work we chose $\eta = 1$ and $I_{45} = 1$ as is usual to choose. We note that, η and I can be eliminated from the equations by defining new variables as $\sqrt{\eta I_{45}} \Omega$ and $\mu / (I_{45} \sqrt{\eta})$. Therefore, for different values of η and I , the initial parameters transform as $P_0 \rightarrow P_0 \sqrt{\eta I_{45}}$ and $\mu_0 \rightarrow \mu_0 I_{45} \sqrt{\eta}$ while the others do not change. In [Figure 8](#) we present all possible values for each source on the $\mu_0 - P_0$ plane. We emphasize that the evolution of the inclination angle and the braking index are not affected by the choice of η or I .

Recently, [Xiao & Dai \(2017, 2019\)](#) calculated the X-ray efficiency factor as a function of luminosity based on an emission mechanism governed by Poynting flux-dominated wind. This implies that the value of η may not be constant during the episodes we consider. Yet given that η depends also on the beaming fraction, employing any possible dependence on the luminosity will not improve our estimates on the initial parameters. Considering the dependence of η on luminosity and beaming will be carried over in a future work and is beyond the scope of the present paper.

4 SUMMARY AND DISCUSSION

We have invoked the ‘millisecond magnetar model’ ([Usov 1992; Duncan & Thompson 1992](#)) to infer the initial parameters of nascent magnetars from the X-ray afterglow light curves of GRBs.

We have presented an explicit approximate analytical solution of the system of equations describing the evolution of spin and inclination angle of a magnetized neutron star. We have shown that this solution is very accurate except for highly orthogonal initial conditions ($\alpha_0 > 70^\circ$).

We have fitted, via a Bayesian procedure, the light curves of 6 GRB afterglows by using the analytical solution to determine the evolution of the period, inclination angle,

¹ http://www.swift.ac.uk/xrt_curves/

magnetic dipole moment and the braking index. The spin and magnetic parameters we obtained are consistent with the initial parameters suggested for the ‘millisecond magnetar model’.

We have shown that the inclination angle, just like the spin period, varies rapidly within the time-frame of the X-ray afterglows. This is compatible with the recent result we have obtained that the inclination angles of magnetars align rapidly within the first ~ 10 days (Paper I). As a consequence of the alignment and magnetic field decay the braking index is greater than three ($n > 3$) and varies rapidly confirming the results of (Paper I). According to this picture the constant braking indices inferred by Lasky et al. (2017) and Lü et al. (2019) are effective average values.

Magnetohydrodynamics simulations employed for nascent magnetars have shown that these stars continue their lives with magnetar strength magnetic fields if the star has a high rotation period ($P < 6$ ms) and small inclination angle ($\alpha < 45^\circ$) (Geppert & Rheinhardt 2006). Although we can not give a limit on period due to its dependence on the poorly constrained η parameter, all inclination angle values in our sample are smaller than 45° i.e. compatible with the theoretical prediction of Geppert & Rheinhardt (2006). We thank Prof. Geppert for bringing into our attention this interesting prediction.

The ‘millisecond magnetar model’ is often invoked as an explanation to the ‘plateau phase’ observed in some X-ray afterglows. We have shown that the magnetic field of a nascent magnetar may decline immediately after its birth. Most of the models in the literature (e.g. Colpi et al. (2000)) consider the long-term evolution of magnetic fields of magnetars with solid crusts. This is a quasi-equilibrium stage. Evolutionary time-scales observed in these simulations are hundreds of years. The brief episode we consider in this paper is very soon after the initial generation and enhancement of the field by magnetohydrodynamics instabilities where the quasi-equilibrium stage has not yet been achieved and the field may decay more rapidly (Geppert & Rheinhardt 2006; Beniamini et al. 2017). As a result the spin-down power of the magnetar decreases more rapidly than it would if magnetic field remained constant, and thus an extended ‘plateau phase’ may not be realized. According to this picture the systems with the extended ‘plateau phase’ host magnetars with relatively longer field decay time-scales. This suggests that the relevance of the ‘millisecond magnetar model’ may not be restricted to the GRB afterglows with a plateau phase.

ACKNOWLEDGEMENTS

This work made use of data supplied by the UK Swift Science Data Centre at the University of Leicester (http://www.swift.ac.uk/xrt_curves/). SŞM acknowledges post-doctoral research support from İstanbul Technical University. SŞM and KYE acknowledges support from TÜBİTAK with grant number 118F028.

REFERENCES

Beniamini P., Giannios D., Metzger B. D., 2017, *MNRAS*, **472**, 3058
 Bloom J. S., Frail D. A., Sari R., 2001, *AJ*, **121**, 2879

- Colpi M., Geppert U., Page D., 2000, *ApJ*, **529**, L29
 Cook G. B., Shapiro S. L., Teukolsky S. A., 1994, *ApJ*, **423**, L117
 Costa E., et al., 1997, *Nature*, **387**, 783
 Dai Z. G., Lu T., 1998a, *Physical Review Letters*, **81**, 4301
 Dai Z. G., Lu T., 1998b, *A&A*, **333**, L87
 Davis L., Goldstein M., 1970, *ApJ*, **159**, L81
 Duncan R. C., Thompson C., 1992, *ApJ*, **392**, L9
 Evans P. A., et al., 2007, *A&A*, **469**, 379
 Evans P. A., et al., 2009, *MNRAS*, **397**, 1177
 Foreman-Mackey D., Hogg D. W., Lang D., Goodman J., 2013, *PASP*, **125**, 306
 Foreman-Mackey D., et al., 2018, emcee, doi:10.5281/zenodo.1436565, <http://doi.org/10.5281/zenodo.1436565>
 Frail D. A., et al., 2001, *ApJ*, **562**, L55
 Geppert U., Rheinhardt M., 2006, *A&A*, **456**, 639
 Goldreich P., Julian W. H., 1969, *ApJ*, **157**, 869
 Haensel P., Potekhin A. Y., Yakovlev D. G., 2007, *Astrophys. Space Sci. Libr.*, **326**, pp.1
 Hones Jr. E. W., Bergeson J. E., 1965, *J. Geophys. Res.*, **70**, 4951
 Kargaltsev O., Durant M., Pavlov G. G., Garmire G., 2012, *ApJS*, **201**, 37
 Kumar P., Zhang B., 2015, *Physics Reports*, **561**, 1
 Lasky P. D., Leris C., Rowlinson A., Glampedakis K., 2017, *ApJ*, **843**, L1
 Lewis A., Handley W., Xu Y., Torrado J., Higson E., 2018, Get-Dist, doi:10.5281/zenodo.1415428, <http://doi.org/10.5281/zenodo.1415428>
 Lü H.-J., Lan L., Liang E.-W., 2019, *ApJ*, **871**, 54
 Lyutikov M., Blandford R., 2003, ArXiv Astrophysics e-prints, Michel F. C., Goldwire Jr. H. C., 1970, *Astrophys. Lett.*, **5**, 21
 Philippov A., Tchekhovskoy A., Li J. G., 2014, *MNRAS*, **441**, 1879
 Piran T., 2005, *Rev. Mod. Phys.*, **76**, 1143
 Price-Whelan A. M., et al., 2018, *AJ*, **156**, 123
 Spitkovsky A., 2006, *ApJ*, **648**, L51
 Usov V. V., 1992, *Nature*, **357**, 472
 Xiao D., Dai Z.-G., 2017, *ApJ*, **846**, 130
 Xiao D., Dai Z.-G., 2019, *ApJ*, **878**, 62
 Zhang B., Mészáros P., 2004, *International Journal of Modern Physics A*, **19**, 2385
 Şaşmaz Muş S., Çıkıntoğlu S., Aygün U., Ceyhun Andaç I., Ekşi K. Y., 2019, *ApJ*, **886**, 5

This paper has been typeset from a $\text{\TeX}/\text{\LaTeX}$ file prepared by the author.

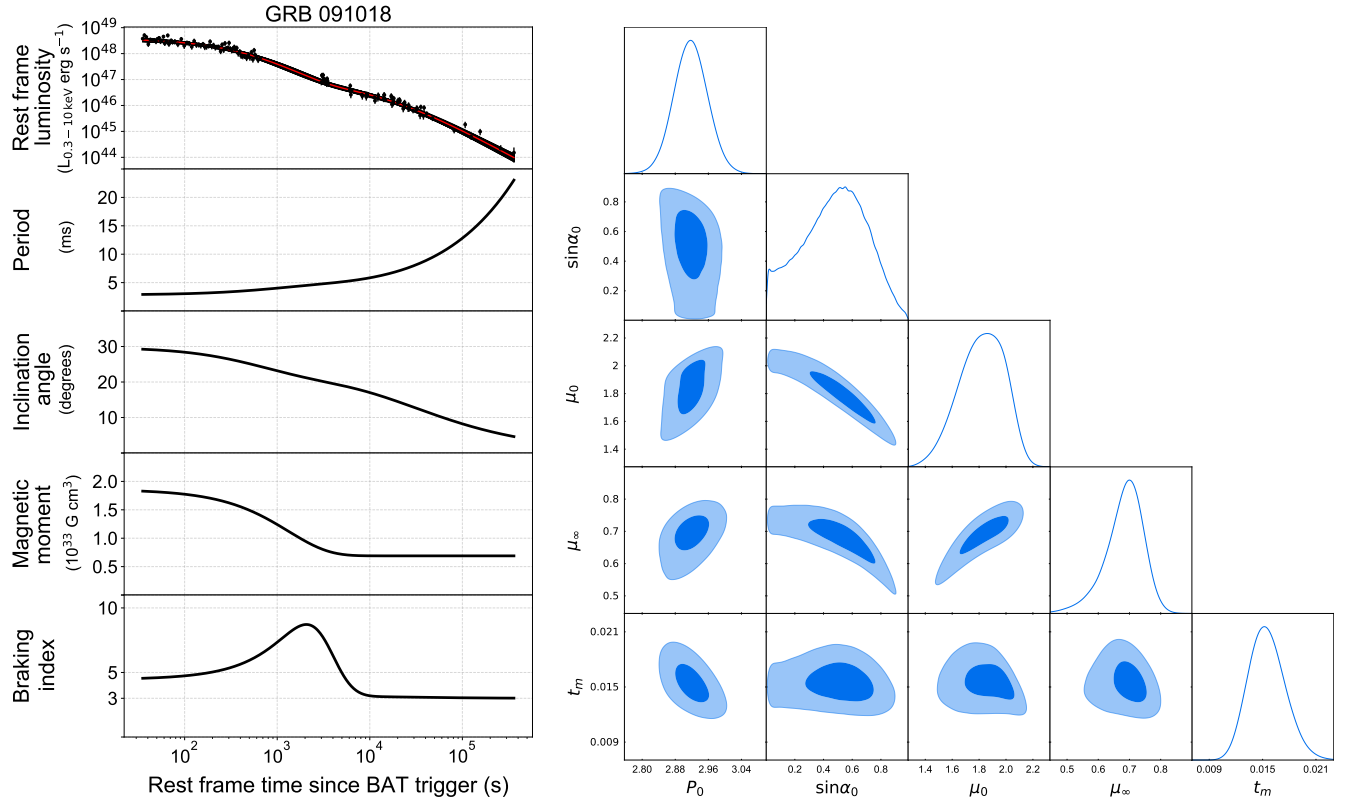


Figure 2. Left: Evolution of luminosity, period, inclination angle, magnetic dipole moment and braking index of putative nascent magnetar in GRB 091018. The red line in the upper panel represents the luminosity model obtained from the median value of all samples. Solid black lines represent randomly chosen 500 models from the posterior distribution. Right: 2D joint (with 1 and 2 sigma contours) and 1D marginalized posterior probability distributions of the parameters plotted with `getdist` package (Lewis et al. 2018).

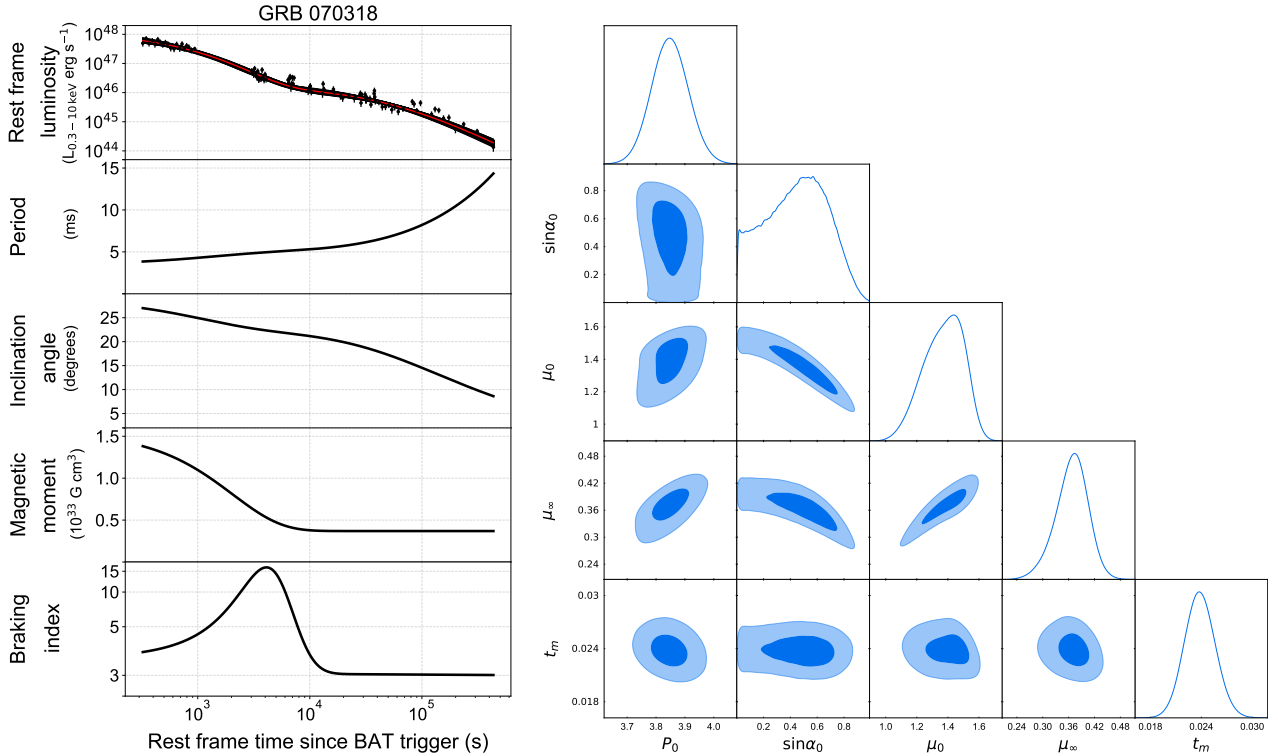


Figure 3. Same as Figure 2 but for GRB 070318.

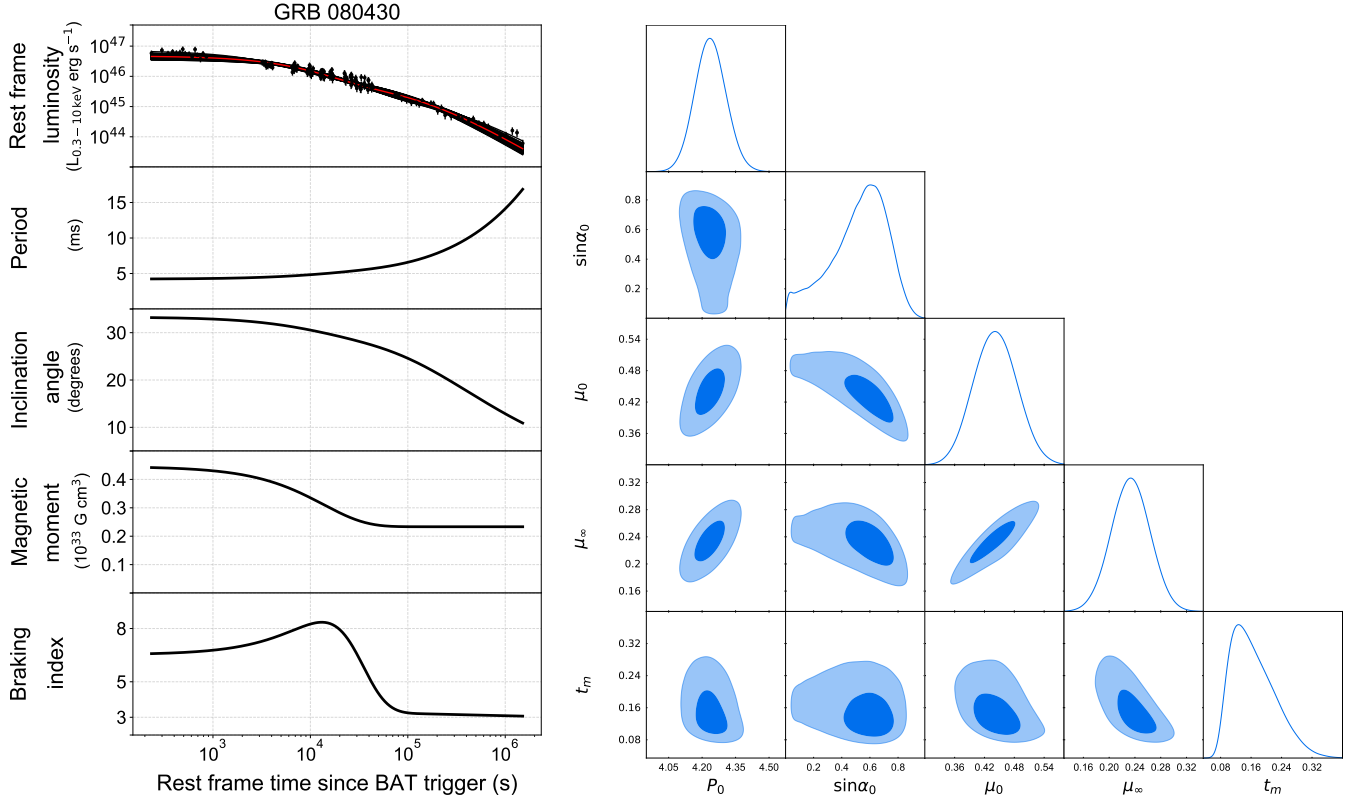


Figure 4. Same as Figure 2 but for GRB 080430.

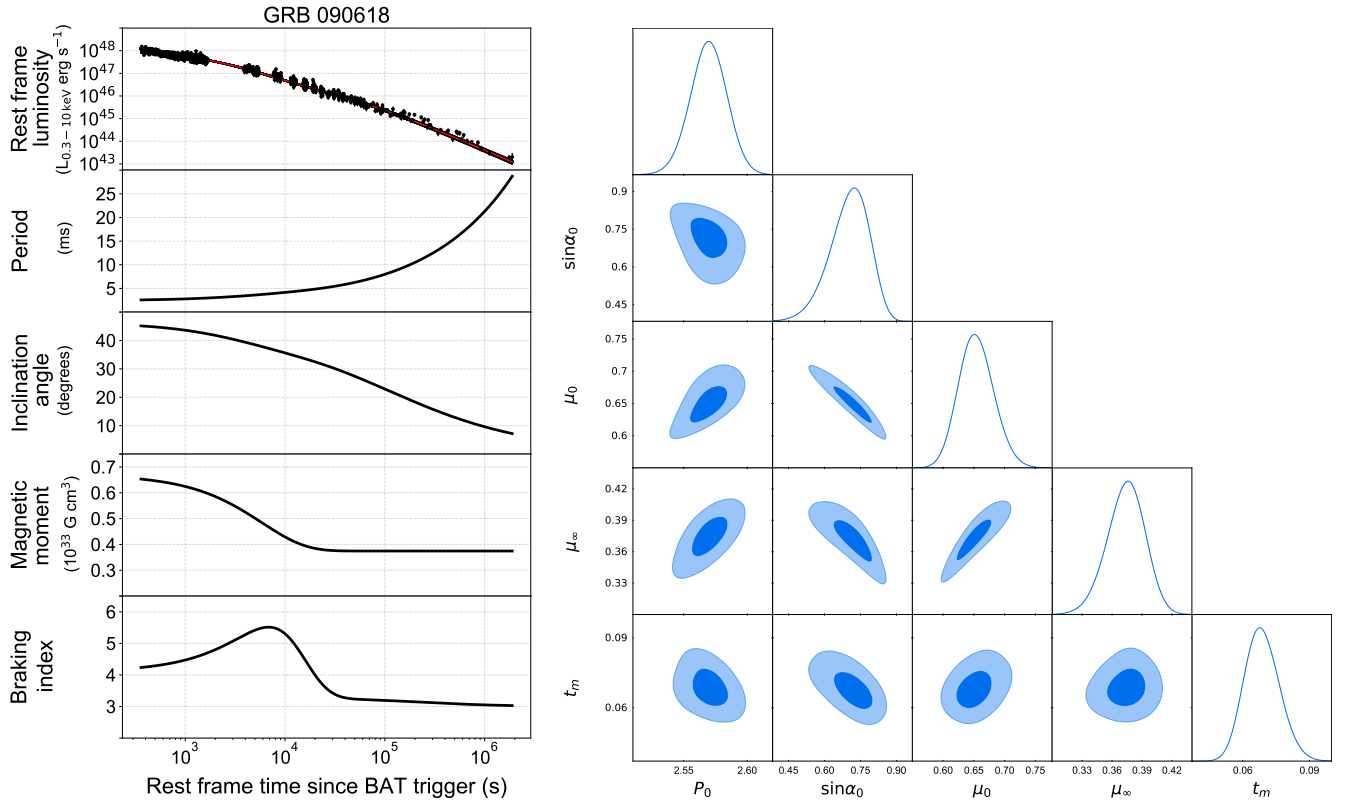


Figure 5. Same as Figure 2 but for GRB 090618.

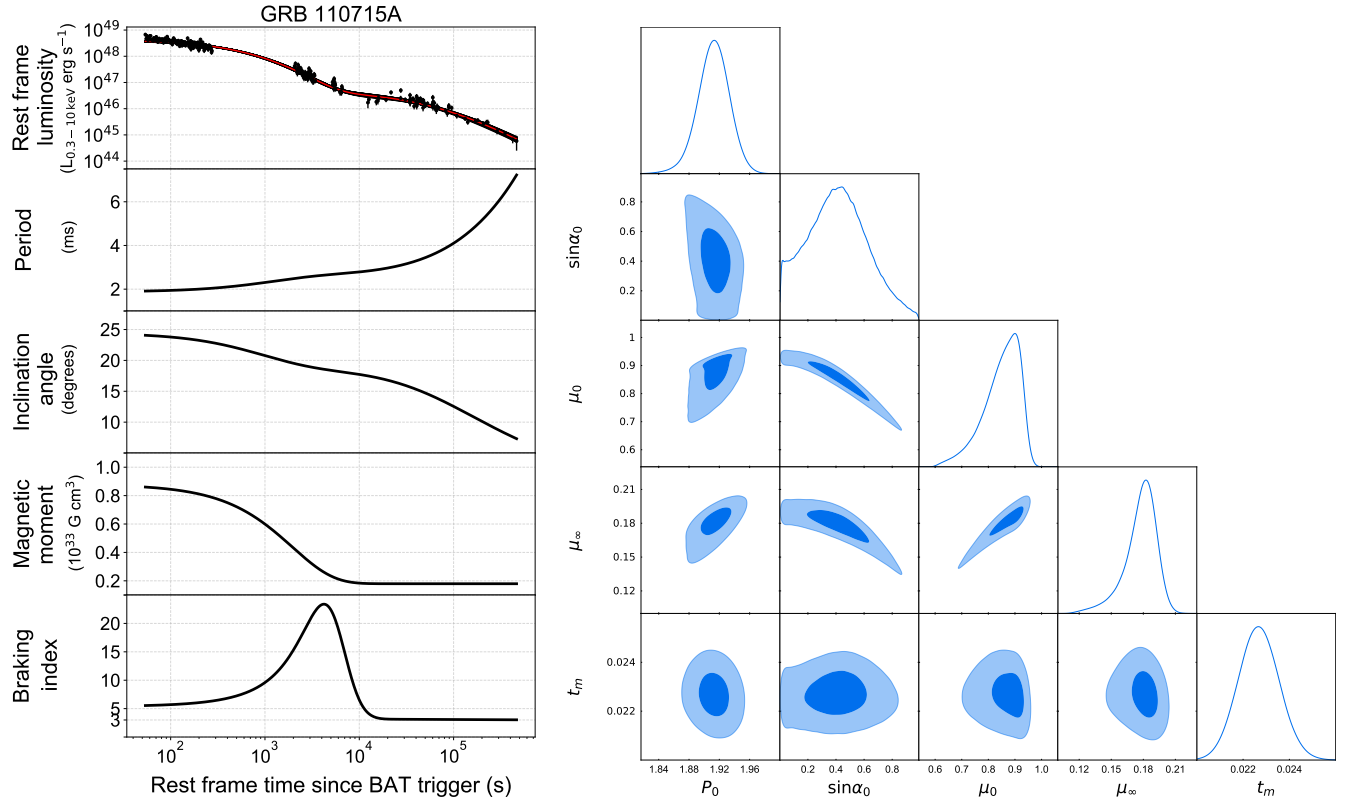


Figure 6. Same as Figure 2 but for GRB 110715A.

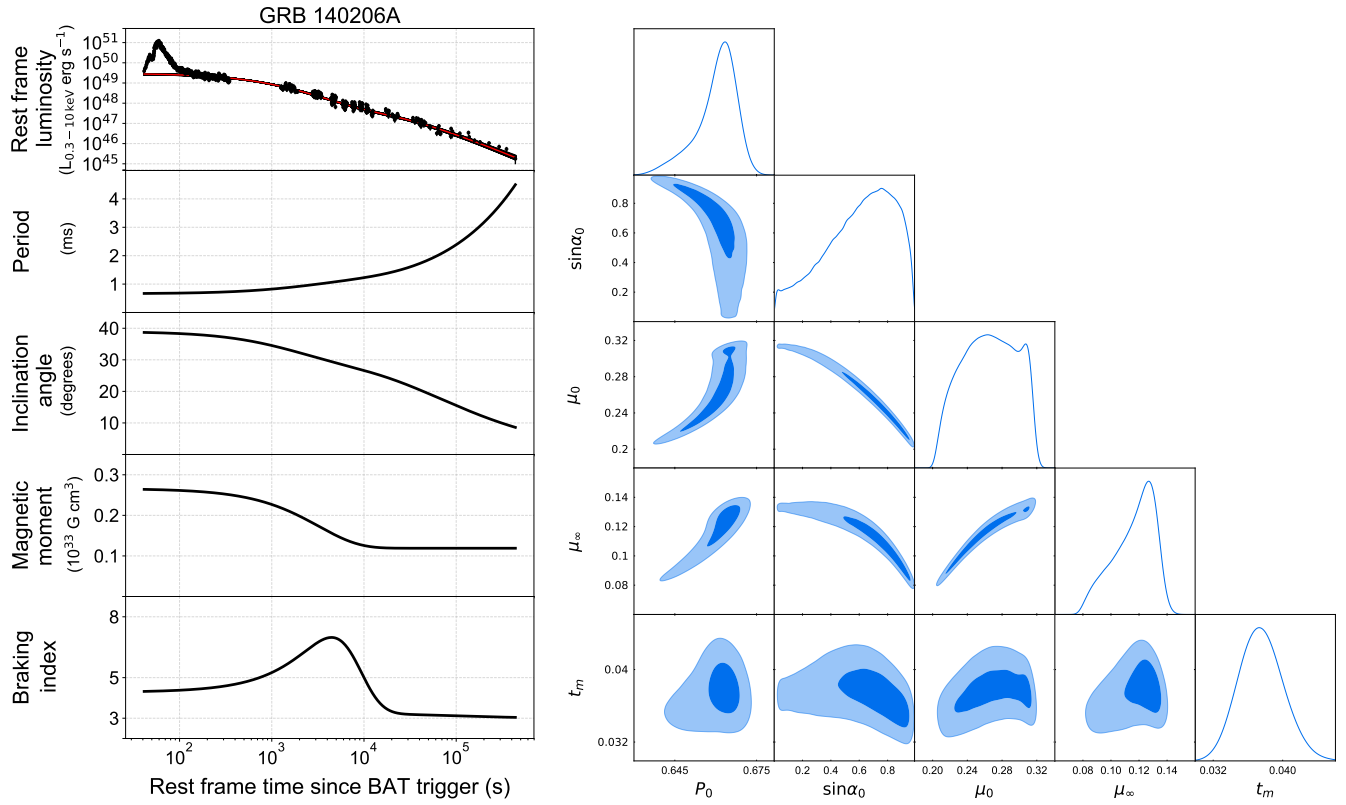


Figure 7. Same as Figure 2 but for GRB 140206A. We excluded the flare data (coloured in green) that comes after the first data point of the presented light curve.

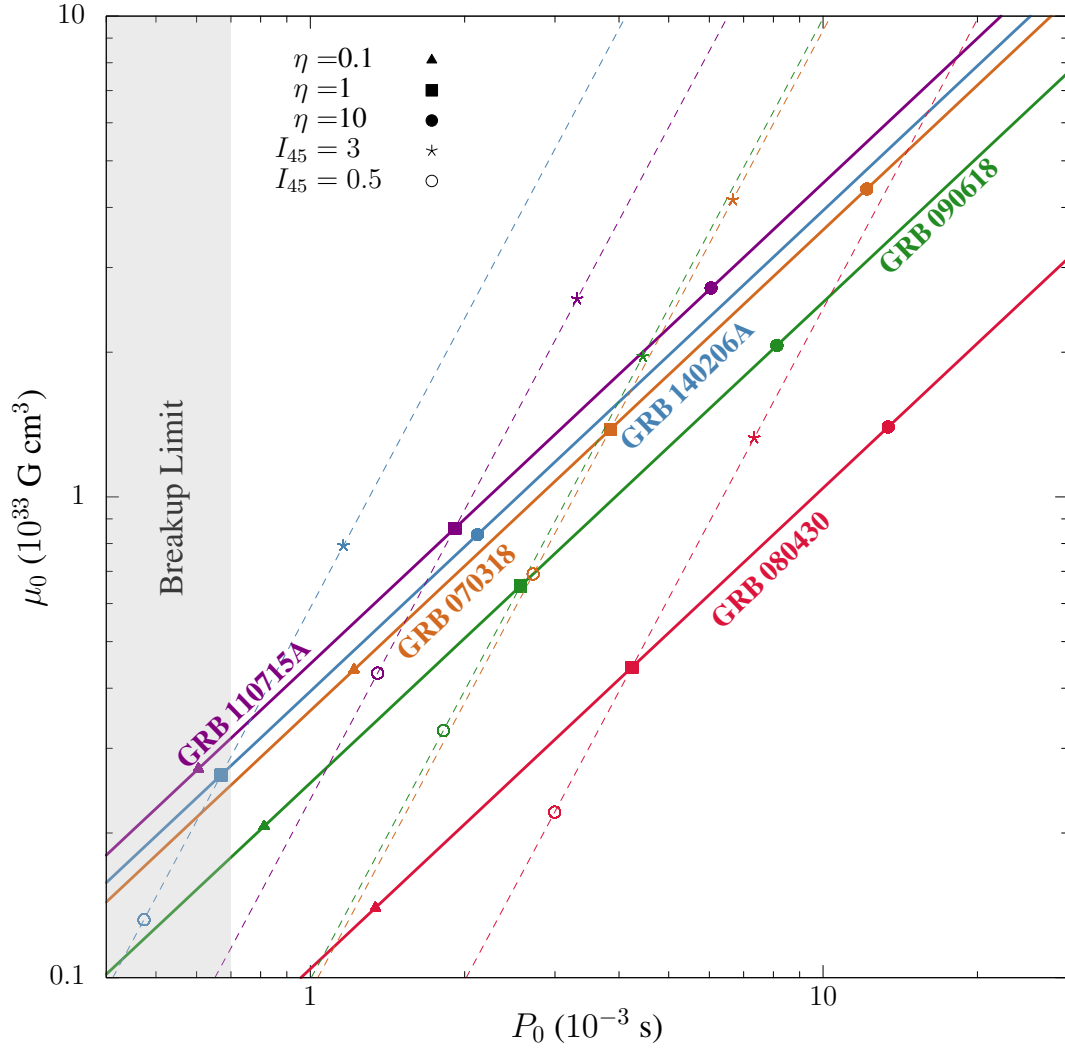


Figure 8. Possible values of the initial period and the initial magnetic dipole moment for different values of η and I_{45} . On solid lines, η varies and I_{45} fixed at 1. On dashed lines, η fixed at 1 and I_{45} varies. The grey shaded area is the possible minimum period range of various equation of states (Cook et al. 1994).